Thermophilic Xylanase from *Thermomyces lanuginosus*: High-Resolution X-ray Structure and Modeling Studies[†,‡]

Karl Gruber,[§] Gerd Klintschar,[§] Marianne Hayn,[||] Anton Schlacher,[⊥] Walter Steiner,[⊥] and Christoph Kratky*[,§]

Institut für Physikalische Chemie, Universität Graz, Heinrichstrasse 28, A-8010 Graz, Austria, Institut für Biochemie, Universität Graz, Schubertstrasse 1, A-8010 Graz, Austria, and Institut für Biotechnologie, Technische Universität Graz, Petersgasse 12, A-8010 Graz, Austria

Received April 17, 1998; Revised Manuscript Received July 6, 1998

ABSTRACT: The crystal structure of the thermostable xylanase from *Thermomyces lanuginosus* was determined by single-crystal X-ray diffraction. The protein crystallizes in space group $P2_1$, $a = 40.96(4)$ Å, $b = 52.57(5)$ Å, $c = 50.47$ (5) Å, $\beta = 100.43(5)°$, $Z = 2$. Diffraction data were collected at room temperature for a resolution range of 25−1.55 Å, and the structure was solved by molecular replacement with the coordinates of xylanase II from *Trichoderma reesei* as a search model and refined to a crystallographic *R*-factor of 0.155 for all observed reflections. The enzyme belongs to the family 11 of glycosyl hydrolases [Henrissat, B., and Bairoch, A. (1993) *Biochem. J. 293*, 781−788]. pK_a calculations were performed to assess the protonation state of residues relevant for catalysis and enzyme stability, and a heptaxylan was fitted into the active-site groove by homology modeling, using the published crystal structure of a complex between the *Bacillus circulans* xylanase and a xylotetraose. Molecular dynamics indicated the central three sugar rings to be tightly bound, whereas the peripheral ones can assume different orientations and conformations, suggesting that the enzyme might also accept xylan chains which are branched at these positions. The reasons for the thermostability of the *T. lanuginosus* xylanase were analyzed by comparing its crystal structure with known structures of mesophilic family 11 xylanases. It appears that the thermostability is due to the presence of an extra disulfide bridge, as well as to an increase in the density of charged residues throughout the protein.

Xylanases (EC 3.2.1.8) belong to the large group of glycosyl hydrolases. They catalyze the degradation of xylan, the most abundant hemicellulose synthesized in the biosphere. Xylans are heteropolysaccharides consisting of a backbone of 1,4-linked xylose monomers and are typically branched with arabinose, glucuronic acid, and acetate substituents at the 2- and 3-position of xylose (*1*). The degree of backbone polymerization and the nature and number of substituents depend on the biological source of the xylan.

Biologically, xylanases are synthesized by microorganisms and secreted to degrade surrounding xylan as food supply. In recent years, xylanases are increasingly used in industrial processes in the food and feed industries (*2*, *3*) and in the pulp and paper industries (*4*). There, xylanases hold the promise of reducing the amount of chlorine chemicals for the pulp-bleaching process. Considerable efforts are devoted to identify new xylanases or to improve the properties of existing ones in order to meet the requirements of industrial paper mills. While chlorine-free bleaching is carried out at very low pH, chlorine bleaching is preceded by a hot, caustic treatment of the wood. Desirable properties of a biotechnologically useful xylanase, therefore, include stability and activity at elevated temperatures and extreme pH values.

Efforts to improve the thermostability of a *Bacillus circulans* xylanase by introducing extra inter- and intramolecular disulfide bridges via site-directed mutagenesis (*5*) were only partly successful: while the introduction of S−S bridges always improved the thermostability of the protein (as judged from the residual enzymatic activity following thermal treatment), only one of the tested disulfide bridges enhanced the activity of the enzyme at elevated temperatures. An industrially relevant xylanase from *Bacillus* strain D3 has recently been described (*6*). Its thermostability was ascribed to the presence of six surface aromatic residues, arranged as sticky patches, that should induce aggregation at high protein concentrations.

Enzymatic cleavage of the glycosidic bond may follow two different mechanisms resulting either in overall retention or inversion of the anomeric configuration (*7*). In both cases, the reaction proceeds via general acid catalysis requiring a proton donor and a nucleophile. Accordingly, the first step in the reaction sequence consists of a protonation of the glycosidic oxygen. In the case of the inverting mechanism, a water molecule (activated by the nucleophile) attacks the anomeric carbon atom from the backside, leading to inversion of the absolute configuration. The retaining mechanism, on the other hand, involves two consecutive inverting nucleophilic attacks (first by the nucleophile and subsequently by

[†] This work was supported by the Austrian national science foundation (FWF) through the Spezialforschungsbereich Biokatalyse and through Project 11599 and by the Jubiläumsfonds der österreichischen Nationalbank (Project 4991 to C.K.).

[‡] Crystallographic coordinates have been deposited in the Brookhaven Protein Data Bank (accession no 1yna).

* Author to whom correspondence should be addressed. Tel: +43 316 380 5417. Fax: +43 316 380 9850. E-mail Christoph.Kratky@Kfunigraz.ac.at.

[§] Institut für Physikalische Chemie.

[||] Institut für Biochemie.

[⊥] Institut für Biotechnologie.

S0006-2960(98)00864-2 CCC: $15.00
Published on Web 09/05/1998

a water molecule) resulting in overall retention of the anomeric configuration. It is still an open question, whether the nucleophile forms a covalent bond to the anomeric carbon or if its negative charge only stabilizes the positive charge of the reaction intermediate (*8*).

At least three different types of active-site topologies are known to exist in glycosyl hydrolases (*9*). Pockets are optimal for monosaccharidases, and enzymes adapted to substrates with a large number of available chain ends. A tunnel was observed in cellobiohydrolases (*10*). This topology requires the polysaccharide chain to be threaded through, which is optimal for fibrous substrates such as native cellulose. The tunnel appears to be a special case of the third topology, the cleft or groove. Clefts allow the binding of several consecutive sugar units in linear or branched polymeric substrates, and they are commonly observed in endo-acting polysaccharidases.

So far, at least 50 sequences of xylanases have been published. Hydrophobic cluster analysis and sequence alignment showed them to be spread among two families of glycosyl hydrolases (*11*, *12*), belonging either to family 10 or 11 (former families F and G). For members of both families, 3D structures have been determined by X-ray diffraction: the xylanases from *Streptomyces lividans* (*13*), *Pseudomonas Fluorescens* (*14*, *15*), *Cellulomonas fimi* (*16*), and *Clostridium thermocellum* (*17*) belong to family 10, the ones from *B. circulans*, *Trichoderma harzianum* (*18*), *Bacillus* strain D3 (*6*), and the two xylanases (I and II) from *Trichoderma reesei* (*19*, *20*) belong to family 11.

The present report deals with the xylanase from *Thermomyces lanuginosus*, a thermophilic fungus previously called *Humicola lanuginosa*. The xylanase has a molecular mass of about 21 kDa and is a member of family 11 of glycosyl hydrolases, as judged from its primary structure (*21*). This class of enzymes is known to catalyze hydrolysis with retention of the anomeric configuration (*9*). The pI of the enzyme is 4.1 and it is most active at 70 °C and a pH of 6.5. The enzyme has been extensively studied with regard to its production and biotechnological use (*22*−*26*), and recently its gene was cloned and characterized (*21*). Here, we describe the results of a crystal structure analysis of this enzyme and a comparison of its structure with other structures of family 11 xylanases. The roles of individual residues involved in catalysis and the number of subsites in the active-site cleft are determined by modeling studies. Estimates of the pK_a values of ionizable groups are calculated and discussed in view of the proposed catalytic mechanism. Since this is a thermostable xylanase, its 3D structure is compared to available structures of the same class from mesophilic organisms in view of possible factors conferring thermostability. These results should be useful for future mutagenesis studies aimed at improving the thermostability of this biotechnologically important class of enzymes.

MATERIALS AND METHODS

Purification and Crystallization of the Enzyme. The xylanase was purified from culture filtrate as decribed recently (*21*). The molecular mass is 21 kDa, as deduced from the genomic DNA sequence after cleavage of a signal peptide consisting of the first 31 residues. The apparent molecular mass from SDS−PAGE was determined as 24−26 kDa (*24*). There is no evidence for glycosilation.

For crystallization, the lyophilized protein was dissolved and dialyzed against 10 mM HEPES buffer pH = 7.5 for 48 h. Crystals were obtained at 4 °C in hanging drops: 8−12 μL droplets contained about 4 mg/mL xylanase, 2.5−5.0% w/v PEG-6000 and 0.1% w/v *n*-octyl-β-glucoside in 100 mM citrate buffer pH = 4.0. They were equilibrated against a reservoir solution with a 2-fold higher concentration of PEG-6000 in citrate buffer. Seeding after about 1 day of equilibration was necessary for suitable crystals to appear. The elongated crystals reach a maximum length of 1 mm, with a typical size of 0.5 × 0.1 × 0.1 mm.

Data Collection. Diffraction data were collected at two different temperatures using a Siemens rotating anode X-ray source (CuK_α radiation, 1.542 Å), equipped with a Siemens X-1000 multiwire area detector mounted on a three circle goniometer.

A first data set—which was subsequently used for the structure solution—was collected at −180 °C from a crystal with approximate dimensions of 0.3 × 0.1 × 0.1 mm. The crystal was shock-cooled after soaking in a cryoprotectant containing 30% v/v glycerol. Crystals are monoclinic, space group $P2_1$, with cell dimensions [at 93(2) K] of a = 40.32 (6) Å, b = 51.58(8) Å, c = 50.24(6) Å, and β =100.1(1) (V = 102 850 Å^3). Reflections numbering 11 730 were measured (10 cm crystal-to-detector distance, ω-scans, 0.25° oscillation angle) in the resolution range 19.8−3.5 Å, yielding 2546 unique reflections (R_{merge} = 0.112, $\langle I/\sigma(I)\rangle$ = 6.2, average multiplicity = 4.6, completeness = 96.4%).

A room temperature data set (which was used for structure refinement) was subsequently collected from a crystal (0.5 × 0.15 × 0.1 mm) mounted in a sealed capillary: monoclinic, space group $P2_1$, a = 40.96(4) Å, b = 52.57(5) Å, c = 50.47(5) Å, β = 100.43(5), V = 106 880 Å^3 (at 298 K, V/V = 3.8% compared to the 93K cell), V_m = 2.51 Å^3/Da, solvent content approximately 51%. Reflections numbering 81 936 were measured (crystal-to-detector distance 7.5 cm, ω-oscillation range 0.25) between 25.3 and 1.55 Å; 26 211 unique reflections, R_{merge} = 0.075 (0.354 for the highest resolution shell), $\langle I/\sigma(I)\rangle$ = 7.7, mean multiplicity = 3.1, completeness = 83.9% (30.7% for the last shell, >90% for reflections below 1.8 Å), precentage of reflections with $I > 2\sigma(I)$ = 74.2% (22.5%).

Both data sets were indexed and processed with the XDS program (*27*−*29*) and programs of the CCP4 package (*30*).

Structure Solution and Refinement. The structure of the *T. lanuginosus* xylanase was solved by molecular replacement, using the coordinates of xylanase II from *Tr. reesei* (*20*) as a search model (60.5% sequence homology, see Figure 1). The entire molecule with all side chains, excluding the N-terminal residue and the solvent molecules, were input into the molecular replacement computations [program X-PLOR (*31*)]. For the structure factor calculations, the model (approximate size 44 × 40 × 34 Å) was placed into a P1-box of dimensions 90 × 80 × 70 Å. The cross rotation search was limited to an Euler space of $0° \le \alpha \le 360°$, $0° \le \beta \le 90°$, and $0° \le \gamma \le 360°$. The integration range was 5−20 Å; reflections from the low-temperature data set between 10 and 4 Å resolution with $F > 3\sigma(F)$ were used. The highest peak of the rotation function (later confirmed to be the correct solution) was 10.0σ above the mean value, compared to 5.4σ for the second highest peak. The best 68 solutions were selected for a PC

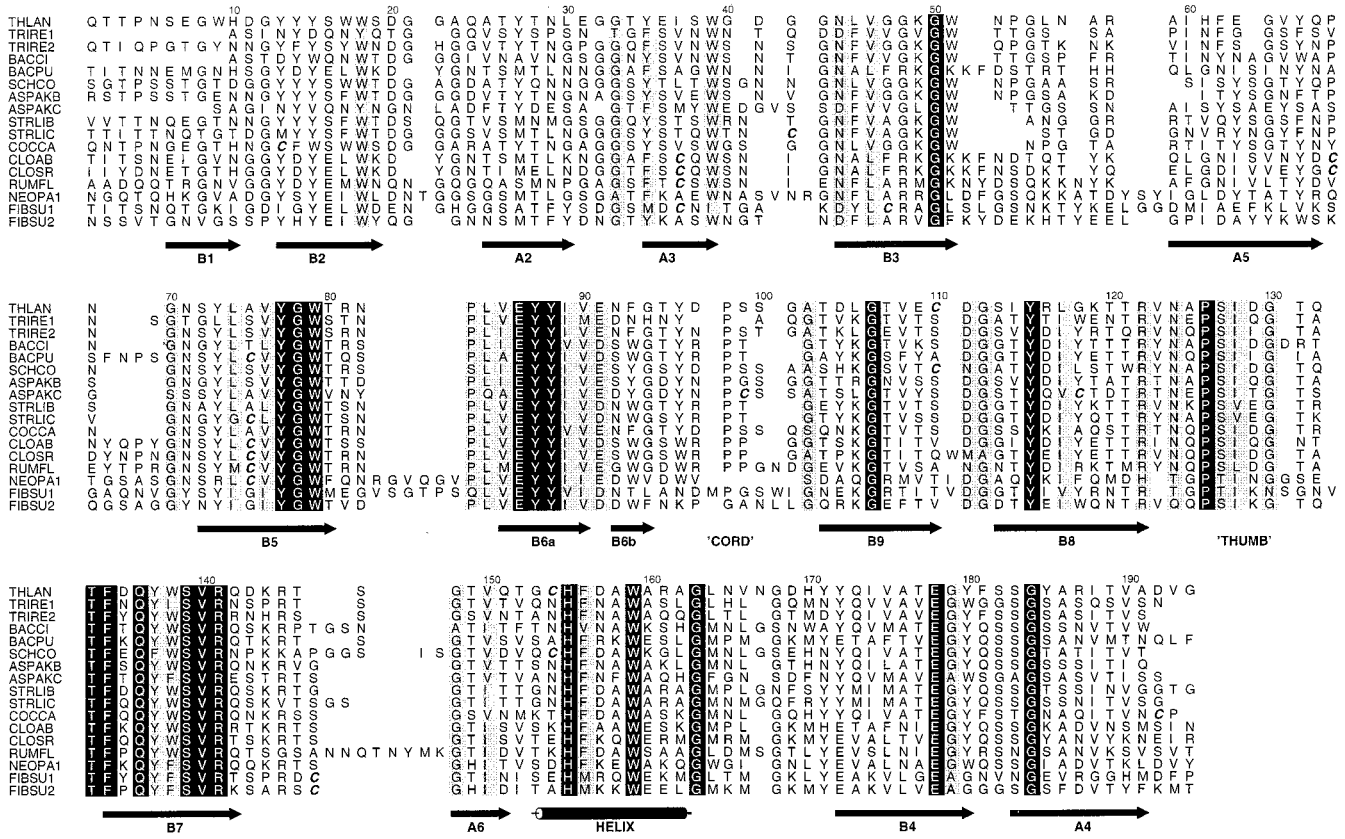

FIGURE 1: Multiple sequence alignment of family 11 xylanases obtained with the program package AMPS (*81*). The sequence alignment is based on a structure alignment of the xylanases from *T. lanuginosus*, *T. reesei*, and *B. circulans*. The figure was prepared with ALSCRIPT (*82*). Shading indicates positions with a conservation index of 8 or greater according to an analysis using AMAS (*83*). Secondary structure elements and residue numbering correspond to the xylanase from *T. lanuginosus*. The sequences are THLAN = *T. lanuginosus*, TRIRE1 and TRIRE2 = xylanases I and II from *T. reesei* (*84*), BACCI = *B. circulans* (*85*), BACPU = *Bacillus pumilis* (*86*), SCHCO = *Schizophyllum commune* (*80*), ASPAKB and ASPAKC = xylanases B (Swissprot entry XYNB_ASPAK) and C from *Aspergillus awamori* (var. kawachi) (*87*), STRLIB and STRLIC = xylanases B and C from *Streptomyces lividans* (*88*), COCCA = *Cochliobolus carbonum* (*89*), CLOAB = *Clostridium acetobutylicum* (*90*), CLOSR = *Clostridium stercorarium* (*91*), RUMFL = *Ruminococcus flavefaciens* (*92*), NEOPA1 = *Neocallimastix patriciarum* (*60*), FIBSU1 and FIBSU2 = *Fibrobacter succinogenes* (*93*). The sequences of the xylanases from *T. harzianum* and *B. subtilis* as well as the second domain of the xylanase from *Neocallimastix patriciarum* were omitted because of their near identity to other sequences in the alignment.

refinement (*32*), yielding two identical solutions with a patterson correlation coefficient of 0.286. The second highest peak was at 0.139 with a distance of about 102°. The best solution was used for a two-dimensional translation search in the *xz*-plane ($0 \le x,z \le 0.5$) with a grid spacing of 1 Å. The calculations were done using data from 10 to 3.5 Å with $F > 3\sigma(F)$, yielding one clear solution (T-function 6.3σ above the mean; *R*-value after rigid-body refinement 0.449). The resulting $3F_o - 2F_c$ map allowed to identify and build the missing and differing side chains, using the program O (*33*). The only exception was the N-termial residue (see below).

At this stage, the high-resolution room-temperature data set became available, and it was used for another rigid-body refinement of the modified MR solution against data with $F > 2\sigma(F)$between 10.0 and 2.0 Å resolution, followed by a slow cooling MD run (*34*) [starting temperature: 4000 K, $R = 0.253$, $R_{free} = 0.311$ (*35*) for 10% of the data]. Several cycles of conventional positional refinement, restrained *B*-factor refinement and manual model building resulted in a final model consisting of 1787 non-hydrogen atoms (1512 protein and 275 solvent atoms, 130 with a fixed occupancy of 0.5). This model gave an *R*-value of 0.184 ($R_{free} = 0.225$) for all data up to 1.6 Å resolution with $F > 2\sigma(F)$. The Engh−Huber parameter set (*36*) was used throughout. Very weak density was observed for the N-terminal residue, which was best modeled by a pyrrolidone-carboxylic acid (PCA) as in xylanase II from *T. reesei* (*20*).

The X-PLOR-model was further refined with the program SHELXL (*37*), first by conjugate gradient minimization and then using a blocked-matrix least-squares technique. The quantity minmized was $\sum w(F_o^2 - F_c^2)^2$ with $w = 1/[\sigma^2(F_o^2) + (0.1P)^2]$, $P = [\max(F_o^2,0) + 2F_c^2)/3$ using all reflections to a resolution of 1.55 Å.

Restraints for 1,2- and 1,3-distances were applied with effective standard deviations of 0.015 Å. Phenyl, imidazolyl, and indole rings as well as guanidinium, carboxylate, and amide groups were restrained to be planar with a σ of 0.1 Å^3 (chiral volume). A larger σ (0.3 Å^3) was used for restraining the planarity of the peptide groups.

Individual isotropic displacement parameters [*U*-instead of *B*-values, following the recommendation of the International Union of Crystallography (*38*), $B = 8\pi^2U$] were refined for the non-hydrogen atoms. The *U*-values were restrained to be similar for atoms close in space ($\sigma = 0.025$ Å^2, cutoff, 1.7 Å). Hydrogen atoms were included at calculated positions. During the refinement they were treated as riding on the respective non-hydrogen atoms. The

U-values of hydrogens were set to 1.2 or 1.5 times (methyl- and hydroxy-hydrogen atoms, respectively) the *U*-value of the central atom.

Prior to the SHELXL refinement, the occupancies of all water molecules were reset to 1.0 and fixed. Water molecules were excluded from further refinement, when their *U*-values exceeded 0.75 Å^2. For solvent molecules, anti-bumping restraints were applied (*37*). The contribution of diffuse solvent to the scattering was accounted for by means of Babinet's principle (*39*): the term $g \exp[-8\pi^2 U(\sin\theta/\lambda)^2]$, $U = 2.0$ Å^2, $g = 5.1$ e$^-$, was subtracted from the real part of the scattering factor for each non-hydrogen atom.

The current model consists of 1649 non-hydrogen atoms (1512 protein and 138 solvent atoms). Refinement of 6598 parameters against 26211 intensity data and 6091 restraints converged at the following values for the reliability indices: $wR^2 = [w(F_o^2 - F_c^2)^2/\sum w(F_o^2)^2]^{1/2} = 0.378$ (for all reflections), $R_1 = ||F_o| - |F_c||/\sum|F_o| = 0.155$ for 19 452 reflections with $F_o > 4\sigma(F_o)$ and 0.193 for all reflections; goodness-of-fit $S = (\sum w[F_o^2 - F_c^2)^2/(n - p)]^{1/2} = 2.81$ ($n = 26\,211$, number of observations; $p = 6598$, number of parameters). Rms-deviations from ideal values [Engh−Huber paramters (*36*)] are 0.008 Å for bond lengths and 1.4 for bond angles. The mean *U*-value is 0.20 Å^2 for main-chain atoms, 0.25 Å^2 for side-chain atoms, and 0.48 Å^2 for the solvent.

The atomic coordinates of the refined model have been deposited with the Brookhaven Protein Data Bank (accession code 1yna).

Structure Validation. The validity of the structure was checked using the program PROCHECK (*40*). In this analysis, values for stereochemical parameters typical for a structure at a resolution of about 1.5 Å were obtained. The overall *G*-factor was 0.0, slightly better than expected (−0.2). Of the residues, 88.6% (except Gly and Pro) have their φ- and ψ-angles located in the core regions of a Ramachandran plot, with no residues observed in the generously allowed or forbidden parts. Leu45 was labeled in a χ_1/χ_2 plot as being in an unfavorable conformation. The electron density for this residue, however, is very clear, and *U*-values are low (0.13−0.23 Å^2). The distribution of ω-angles was considered by the program potentially unusual (*G*-factor, −0.69). It has a mean value of 178.5° and a standard deviation of 6.1°. Ten residues have ω-angles deviating more than 2σ from the mean value. The largest deviations (>3) are found for Thr80 and Val76. Residues showing significant deviations are clustered in the hinge region of β-sheet B.

Calculation of pK_a Values. The pK_a values of ionizable residues (except tyrosines) were estimated for the native enzyme, for the modeled heptaxylan complex (see below) and for several mutants with single amino acid exchanges. The programs described by Yang et al. (*41*) were used throughout. Hydrogen atoms were generated (including crystallographically observed water molecules) by the molecular dynamics program PMD (*42*). This was followed by a short dynamics run (approximately 5 ps) using version 22 of the CHARMm force field (*43*) and retaining the positions of known non-hydrogen atoms. Structures of mutants were also built with PMD. Eletrostatic potentials were calculated using the finite difference Poisson−Boltzmann (FDPB) method (*44*) as implemented in the program Delphi (*45*). The two values for the bulk dielectric constant were set to 4.0 (protein) and 80.0 (solvent). A salt concentration of 0.14 M (corresponding to a Debye length of 8.0 Å) was used throughout. No explicit water molecules were included. Default values were used for the pK_as of the isolated amino acids in solution, e.g., 3.9 for Asp, 4.3 for Glu, 6.5 for His, 10.8 for Lys, and 12.5 for Arg.

Calculations included contributions of electrostatic interactions as well as desolvation energies (*41*). Since the exact calculation of a titration curve would necessitate the simultaneous computation of the statistical mechanical average over all possible 2^N protonation states, the Tanford-Roxby approximation (*46*) was used for weakly interacting ionizable groups.

Test calculations resulted in pK_a estimates approximating experimentally observed values within one p*K* unit (*41*). Uncertainties arise from approximations of the model (e.g., the use of only two bulk dielectric constants for protein and solvent) as well as from the fact that different conformations may be present in the crystal and in solution. While the absolute value of the pK_a is thus prone to some error, the directions of shifts upon changes in the protein environment (e.g., by amino acid substitutions) can be predicted more reliably (*41*).

The computational results were validated by comparison with experimental pK_a values for the homologous *Bacillus* xylanase. Thus, the pK_a of the buried and conserved *Bacillus*-His149 was determined as <2.3 by NMR spectroscopy (*47*, *48*), while the calculated value for the equivalent His155 in the *Thermomyces* enzyme was 0.9, also indicating an uncharged imidazole at relevant pH values. Similarly, the pK_a < 2 for Asp83 in the *Bacillus* xylanase (*48*) was reproduced for the equivalent Glu91 (pK_a < 0). Four salt bridges were observed in the structure of the *Thermomyces* xylanase. In all cases, the directions of calculated pK_a shifts for the involved residues were reasonable (upward shifts for bases, downward shifts for acids); their magnitudes, however, were occasionally overestimated in the computations.

Modeling of a Heptaxylan Fragment into the Binding Cleft. Modeling started from the crystal structure of an inactive mutant of the xylanase from *B. circulans* complexed with xylotetraose [PDB code 1bcx (*49*)]. In this structure, electron density for two sugar subunits, occupying subsites −1 and −2, was observed.

The structures of the two xylanases (*B. circulans* and *T. lanuginosus*) were superimposed by minimizing the rms deviation between the α-carbon atoms of Trp18 (Trp9), Glu178 (Glu172), and Glu86 (Glu78, residue numbers in parentheses refer to the *B. circulans* structure, see Figure 1). The three-dimensional arrangement of these three C atoms is highly conserved. The coordinates of the two sugar residues were merged with the coordinates of xylanase from *T. lanuginosus* and minimized by 500 steps of the powell algorithm, with the atoms of the enzyme kept fixed at their positions. Minimization did not lead to significant changes in the conformation of the disaccharide.

Another round of 500 minimization steps was performed with all atoms of the complex unrestrained. Again, no significant changes in the structure were observed. The sugar chain was extended by two residues in the direction of the nonreducing end and three residues in the direction of the reducing end, leading to an enzyme-bound heptasaccharide. The conformation of the newly introduced sugar residues

were manually chosen to cover hydrophobic areas in the binding cleft and to saturate possible partners for hydrogen bonding.

The modeled enzyme−substrate complex was surrounded by a box of 1680 water molecules, using the Molecular Silverware algorithm as implemented in the program SYBYL, and subjected to 10 cycles of a slow cooling protocol. Slow cooling was performed with XPLOR (*31*) using the CHARMm force field (*43*) (version 19) for the protein moiety and a provisional force field parametrization for the heptasaccharide (*50*). Each cycle of slow cooling included setting the temperature to 5000 K and lowering the temperature in steps of 25 K. Simulation for each step was performed for 0.05 ps. The final structure of each cycle was minimized by 500 steps of the Powell algorithm and used as the input for the following cycle.

Non-hydrogen protein atoms were restrained to their positions with a force constant of 20 kcal/mol/Å; non-hydrogen atoms of the two sugar residues at sites −1 and −2 were restrained to their positions with a force constant of 10 kcal/mol/Å. Only two sugar residues at the nonreduceing end, three at the reducing end, and all the water molecules were allowed to move freely.

Extensive molecular dynamics runs were performed to validate the position of protein-bound sugar by repetitive slow-cooling cycles with an unrestrained oligosaccharide (*51*). In the majority of runs, the sugar residues at positions −2, −1, and +1 collapsed to the same binding subsites with very similar conformations of the glycosidic linkages.

RESULTS AND DISCUSSION

We have determined the crystal structure of the xylanase from *T. lanuginosus* by molecular replacement and have refined the coordinates against room-temperature diffraction data extending to a crystallographic resolution of 1.55 Å. The distribution of mainchain torsion angles, the experimental electron density (Figure 2), and the final values of the reliability indices indicate a high-quality structure analysis, with few positional ambiguities for any of the mainchain or side-chain atoms. Overall views of the molecule are shown in Figure 3.

Molecular Structure. The xylanase from *T. lanuginosus* is a compact, globular protein with approximate dimensions of 40 × 38 × 35 Å. The most prominent feature of the structure is a long cleft (about 5−6 Å high and about 8−9 Å deep) spanning the whole molecule and containing the active site.

The structure is dominated by two heavily twisted β-sheets (panels A and B, see Figure 3). Sheet A forms the "outer" surface of the enzyme and consists of five antiparallel strands. Its hydrophilic, solvent-accessible surface contains a large number of serine and threonine residues. Sheet B consists of nine mostly antiparallel strands. One face forms the active site of the enzyme, while the other one is packed against sheet A to form the hydrophobic core of the protein. There is only one α-helix in this structure, which follows strand A6, consists of 10 residues, and is packed against the hydrophobic face of sheet B.

The overall shape of the molecule resembles a right-hand with the two β-sheets and the α-helix forming the "fingers" and the "palm" and two loop regions forming the "thumb"

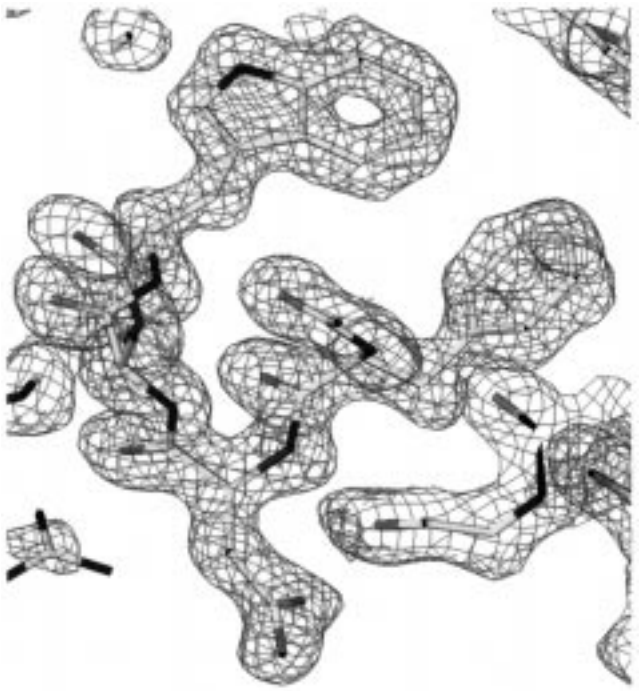

FIGURE 2: Electron density ($3F_o - 2F_c$ map contoured at 1.5) of a portion of the *T. lanuginosus* crystal structure, showing the peptide between Phe156 and Trp159 [generated with program O (*33*)].

and a "cord" (see Figure 3). This picture was first introduced by Törrönen et al. in their description of the structure of xylanase II from *Tr. reesei* (*20*).

The thumb is an 11 residue loop between strands B8 and B7 and exhibits a severely distorted α-ladder hydrogen-bonding pattern. This pattern is interrupted by Asn124, which causes a sharp bend in the loop structure. The amide proton of Ile128 (at the tip of the loop) is in a favorable position for an interaction with the indole ring of Trp79. In NMR measurements of the xylanase from *B. circulans*, the equivalent proton showed a strong upfield shift, indicative of an interaction with the aromatic ring which appears to be necessary for stabilizing the loop (*52*). In the crystal structure, the thumb is well ordered by interactions with sheet B and crystal contacts. Molecular dynamics simulations, however, indicate that it is one of the most flexible parts of the molecule (*51*).

The second extended loop region of special interest is the cord, located between strands B6 and B9. It consists of eight residues and closes the cleft on one side. Two consecutive β-turns form its central part, which results in an S-shaped structure with a nearly planar arrangement of mainchain atoms.

The structures of all family 11 xylanases known so far are similar. Table 1 shows the rms-deviations for C atoms of several xylanase structures [calculated with O (*33*)] together with the number of aligned atom pairs. The maximum deviation of 1.4 Å indicates the close similarity of these structures, especially when the high percentage of C atoms that was used for the least-squares fit is considered. The two central β-sheets are particularly well conserved. Insertions and deletions are mainly found in the loop regions (thumb and cord, see Figure 1). It is noteworthy that the first strand of β-sheet B is lacking in the xylanase from *B. circulans* and xylanase I from *Tr. reesei*. The similarity of

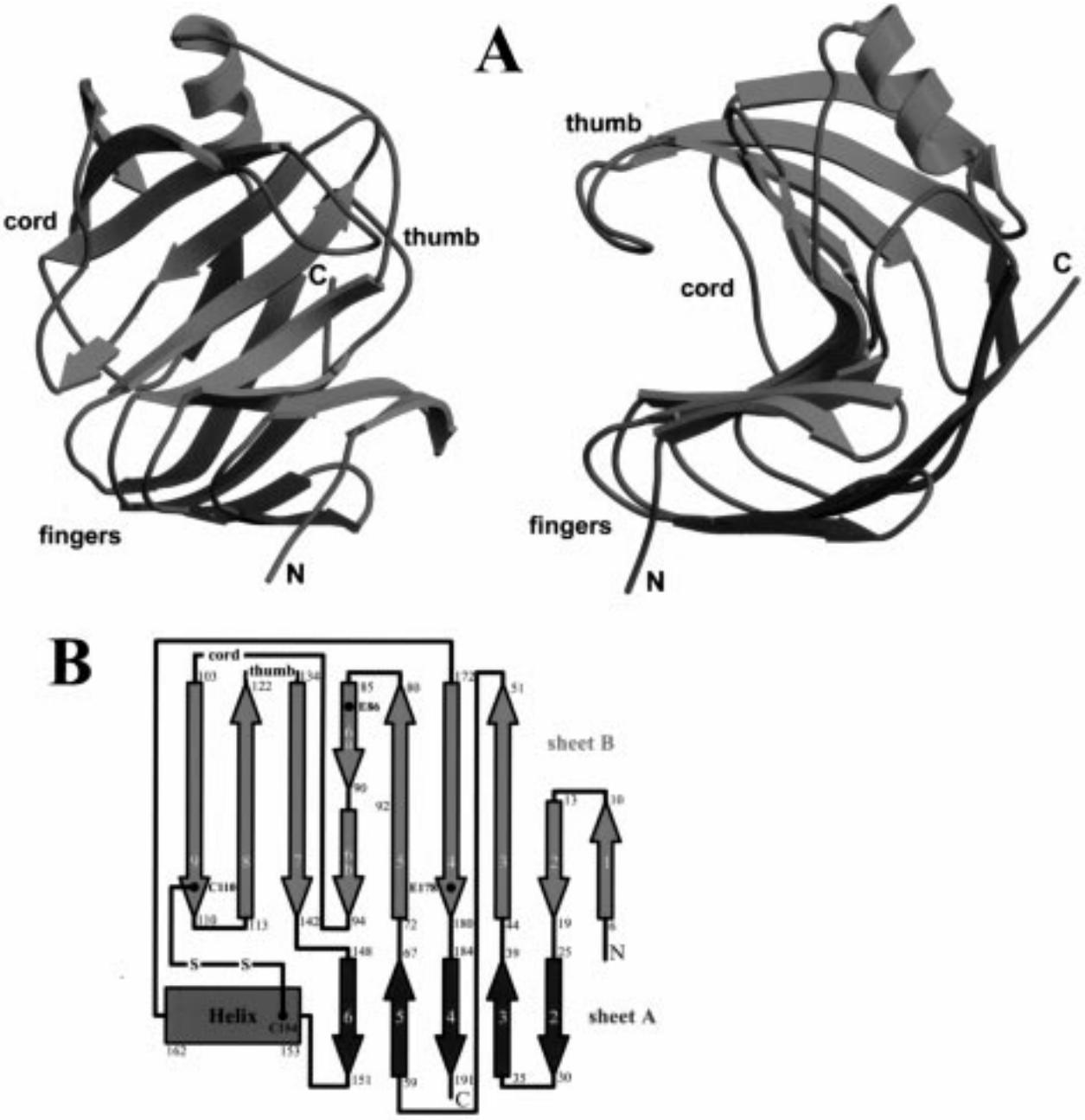

FIGURE 3: (A) Two perpendicular views of the structure of the xylanase from *T. lanuginosus* [generated with programs MOLSCRIPT (*94*) and Raster3D (*95*)]. (B) Topology diagram.

Table 1: Rms-Deviations (Å) and Number of Aligned C_α Atoms (in parentheses) Resulting from a Least Squares Fit Using the Program O (*33*)

	Tr. reesei I	*Tr. reesei II*	*Tr. harzianum*	*B. circulans*
T. Lanuginosus	1.3 (176)	0.9 (188)	1.0 (188)	1.3 (174)
Tr. reesei I		1.1 (172)	1.1 (173)	1.4 (172)
Tr. Reesei II			0.7 (189)	1.4 (173)
Tr. Harzianum				1.1 (177)

family 11 xylanase structures to the 1,3−1,4-glucanase from *Bacillus* (*53*) was noted before (*20*).

As expected, almost all water molecules observed in the crystal structure are located on the surface of the enzyme. One exception is O201, which was found to be deeply buried. It is located at the interface between the turns A3−B3 and B4−A4 and is hydrogen bonded exclusively to mainchain atoms: Gly40 (O, 3.0 Å), Gly43 (O, 2.9 Å; N, 3.3 Å), and Ser182 (N, 3.0 Å). Another buried water molecule is O204, which is sequestered between the α-helix and β-sheet B and is hydrogen bonded to Asp111 (O1, 2.5 Å), Tyr115 (OH, 2.8 Å), and His155 (N2, 2.8 Å). While O201 is only present in the *T. lanuginosus* structure, O204 is conserved among several family 11 xylanases (*18*−*20*, *54*) and appears to play an important role in stabilizing the structure (*47*).

Active Site pK_a Calculations. The active-site cleft is formed by β-sheet B and is well suited to accept a polymeric substrate. Access to the cleft is partly impeded by the cord and the thumb. According to the currently accepted mechanism for retaining glycosidases, two residues are required for catalysis (*7*): a general acid−base and a nucleophile. Typically, aspartate or glutamate residues fulfill these tasks, but there are cases (*55*, *56*) where a tyrosine appears to be involved in transition-state stabilization.

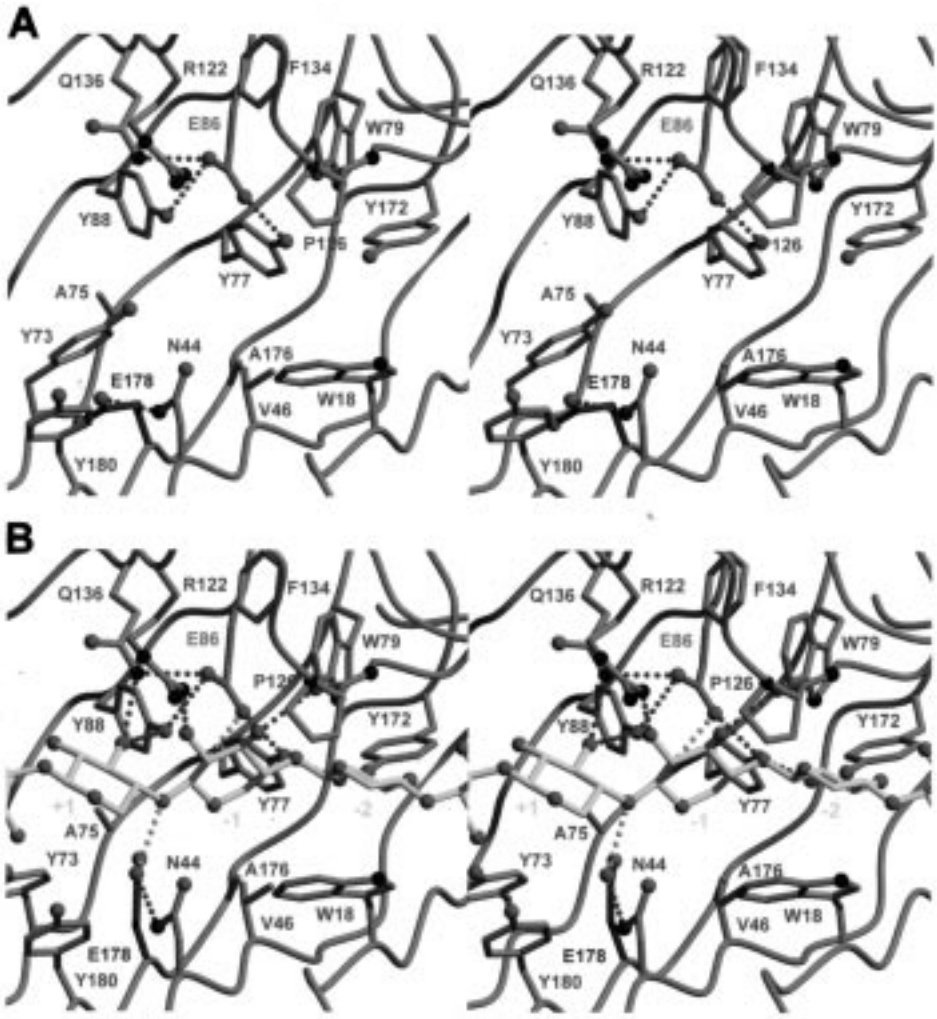

FIGURE 4: (A) Close-up view of the active site of the xylanase from *T. lanuginosus*. Oxygen and nitrogen atoms are shown as red and blue spheres. The putative nucleophile Glu86 is shown in pink, the acid/base catalyst Glu178 in medium blue. Hydrogen bonds are indicated with small green spheres. (B) View of the active site of the modeled complex of the xylanase and a xyloheptaose. Only the three central sugar residues (subsites +1, −1, and −2) are shown in yellow. Possible interactions of the catalytic residues with the substrate are indicated with small orange spheres.

For *Bacillus* xylanases, the active-site residues were determined as Glu78 (nucleophile) and Glu172 (acid−base) by mass spectrometry, using fluorinated xylobiose derivatives (*57*) and mutational studies (*49*). According to a multiple sequence alignment (Figure 1), the equivalent residues in the *Thermomyces* xylanase are Glu86 and Glu178. The mechanism requires Glu86 to be unprotonated and Glu178 to be protonated. In the crystal structure, both residues are almost completely inaccessible to solvent. Glu86, however, is hydrogen bonded to Gln136, Tyr77, and Tyr88 (Figure 4A). Glu178, on the other hand, is located in a rather hydrophobic environment (built up by Tyr73, Gly179, and Tyr180) and accepts only one hydrogen bond from Asn44 (Figure 4A).

The estimated pK_a values also reflect this situation. While the pK_a of Glu86 was found to be virtually unchanged from its value in solution (3.9 vs 4.3), indicative of a negatively charged side chain at neutral pH, the protonated, uncharged state of Glu178 is most likely stabilized in this conformation (pK_a = 9.4). A similar, although smaller shift of the pK_a of the equivalent Glu172 in *B. circulans* xylanase has also been observed in solution by FTIR (*58*) and NMR measurements (*59*). In addition to the hydrogen bonds mentioned above, the close proximity of the guanidinium group of Arg122 (about 5 Å) appears to be another important factor for the stabilization of the negative charge on Glu86. A mutation of this residue to alanine is predicted to result in an increase of the pK_a of Glu86 (to 5.9), while Glu178 would not be affected. This arginine is almost fully conserved among family 11 xylanases (see Figure 1), the only exception being a histidine in the xylanase from *Neocallimastix patriciarum* (*60*), underlining the importance of a positive charge at this position.

The distance between the two active (carboxyl) groups varies depending on the stereochemical course of the reaction. While distances around 5.5 Å are found in retaining glycosidases, larger values (typically around 10 Å) are found for inverting enzymes, because an additional water molecule has to be accommodated between the nucleophile and the anomeric carbon atom of the substrate (*9*). The distance between Glu86 and Glu178 (defined as the mean distance of the carboxylic oxygen atoms) is large (10.7 Å), which appears to be at variance with the sequence-inferred retaining mode of catalysis of this xylanase. The discrepancy, however, can be explained by the unfavorable conformation of the side chain of Glu178, which points away from Glu86

(Figure 4A). This situation is equivalent to the pH 4.5 structure of xylanase II from *Tr. reesei* (*20*) with a distance of 10.9 Å. In this conformation, there is no way for the enzyme to access the substrate and to successfully cleave the glycosidic bond. Since it was observed near the pH-optimum of the *Trichoderma* enzyme, there has to be some conformational change form the "inactive" to a potentially "active" state. This change was indeed observed in the pH 6.5 structure of the same enzyme (approximately 1.5 pH units away from the optimum), which brings closer together the two glutamate residues (distance, 7.2 Å). We believe that the observed pH-induced change may also occur upon substrate binding. Other xylanases with known 3D structure adopt the potentially "active" conformation with short distances between the two catalytic carboxylates: *B. circulans*, 5.9 Å, *Tr. reesei I*, 6.7 Å, and *Tr. harzianum*, 6.4 Å.

Modeling Studies with Xyloheptaose in the Active Site. The xylobiose fragment, which was used as a starting point for further modeling, is situated in the narrowest part of the binding cleft. Trp18 is involved in a stacking interaction with the sugar at subsite −2 (see Figure 4B), a frequently observed type of interaction between protein and carbohydrate. The hydroxy groups of the substrate form hydrogen bonds to a number of residues in the cleft (Figure 4B). Especially noteworthy are three tyrosine residues (Tyr77, Tyr88, and Tyr172) that are nicely lined up on the inside of the active site. Additional interactions were observed with Arg122, Gln136, and the carbonyl oxygen of Pro126. The reducing end of the xylobiose fragment is relatively close to the two catalytic residues. The actual distances between the carboxylic oxygen atoms and their putative sites of attack on the substrate [O1(Glu86)−C1, 4.1 Å, O1(Glu178)−O, 5.5 Å] and the conformation of the side chain of Glu178 are unsuitable for catalysis.

In order for catalysis to occur, a conformational change of the enzyme has to happen. A change of the torsion angles 1−3 of Glu178 and 3 of Glu86 reduces the distances between the two carboxylic groups to 7.1 Å, with a simultaneous change of the Tyr73 conformation necessary to prevent steric clashes. The resulting structure closely resembles the pH 6.5 structure of xylanase II from *Tr. reesei* (*20*). While the distance of 7.1 Å is still longer than expected for a retaining glycosidase, this conformation allows a nucleophilic attack of Glu86 on the anomeric carbon and a hydrogen bond of Glu178 to the glycosidic oxygen atom (Figure 4B).

In the substrate-free enzyme, the conformational changes, especially of Glu178, alter the local environment of both catalytic residues. Glu178 is no longer exclusively surrounded by hydrophobic residues, and the electrostatic interactions between the two side chains increase, resulting in an approach of their pK_a values (5.1 for Glu86 and 6.8 for Glu178). The pK_a values of other residues are not significantly affected by this conformational change. Very similar results were obtained for calculations comparing the pH 4.5 and pH 6.5 structures of xylanase II from *Tr. reesei* (data not shown). For the modeled enzyme−substrate complex, the calculations predict an upward-shift of the pK_a of Glu178 to 8.5, most likely due to the interaction with the glycosidic oxygen of the substrate. This indicates that Glu178 is protonated in the substrate-bound state at relevant pH values, consistent with its putative function in the catalytic mechanism.

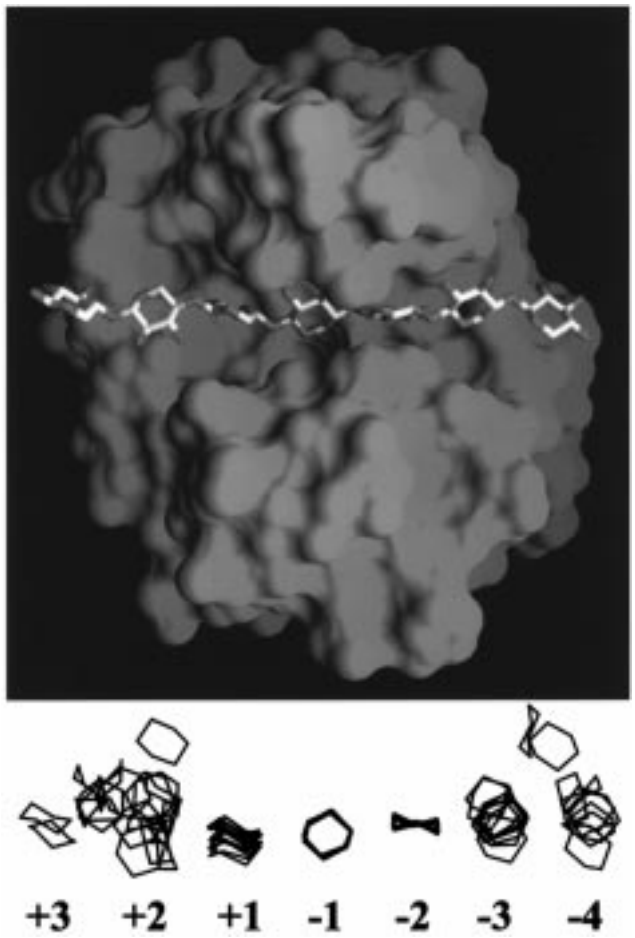

FIGURE 5: Surface representation [GRASP (*96*)] of the *T. lanuginosus* xylanase with the modeled heptaxylan. The lower part of the figure shows a superposition of xylose ring projections from a selection of heptaxylan conformations obtained by molecular dynamics. See the text for details.

Slow cooling runs of the complex with the extended substrate (xyloheptaose) were performed to identify additional subsites in the binding cleft. Throughout these simulations, the xylose residue at subsite +1 remained at its position nearly unchanged, whereas all other sugar residues that were free to move visited multiple sites within the binding cleft. Because of weak coordinate restraints, xylose residues at subsites −2 and −1 remained close to their initial positions. This situation is depicted in Figure 5, showing that those sugar units that do not occupy one of the three central subsites have considerable conformational and orientational flexibility.

It thus seems unlikely that the peripheral subsites are very specific for unbranched xylose residues. As the cleft becomes broader and less specific toward its ends, it should be able to accommodate sugar residues at these locations, which are decorated with different kinds of substituents attached to the backbone.

Thermostability of the T. lanuginosus Xylanase. Due to their technological significance, thermophilic enzymes have attracted much attention, and several of them have been compared structurally with mesophilic counterparts. Several factors conferring thermostability have been identified, including extra disulfide bridges (*54*, *61*−*64*), extra short-range and long-range pairs, and networks of charge−charge interactions (*62*, *65*−*70*), oligomerization (*71*), hydrophobic

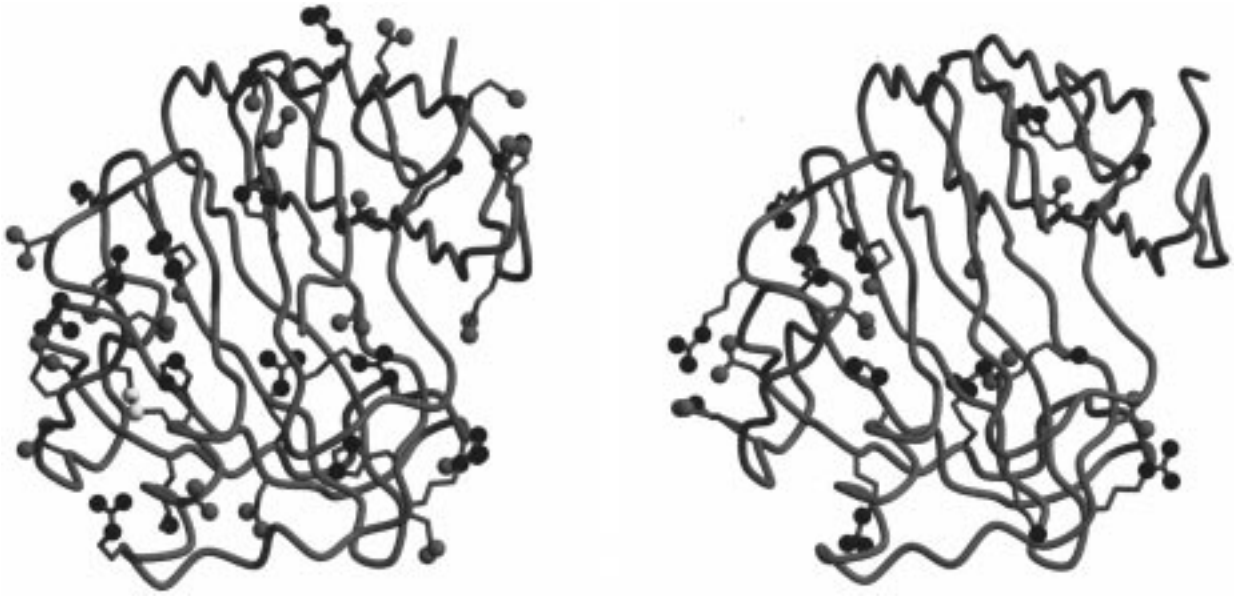

FIGURE 6: Potentially charged residues in the crystal structure of the xylanase from *T. lanuginosus* (left) and of xylanase II from *T. reesei* (right).

interactions (*67*−*69*, *72*), extra proline or glycine substitution sites (*69*, *72*−*74*), protection or shortening of N- and C-terminus (*68*, *69*, *74*), extra pairs or networks of hydrogen bonds (*70*, *72*, *75*−*77*), an increase in polar surface area fraction (*76*, *78*), and other factors. Very often, the combination of several of the above factors was suggested to be responsible for thermostability.

The only thermostable xylanase for which 3D structural data have been reported so far is the one of *Bacillus* strain D3 (*6*). The thermostability of this enzyme, which shows 73% sequence identity to the mesophilic *B. circulans* xylanase, has been accounted to six extra (as compared to *B. circulans*) hydrophobic residues located at the surface of the protein. These residues were proposed to form sticky patches, leading to (stabilizing) enzyme aggregation upon high protein concentrations. However, a comparison of solvent accessibility data of aromatic residues for mesophilic family 11 xylanases (*T. reesei* I, *T. harzianum*, and *B. circulans*) with the *T. lanuginosus* enzyme clearly shows that a similar effect cannot be held responsible for the thermostability of the latter enzyme: the number of solvent exposed aromatic residues [more than 40% exposure, program NAOMI (*79*)] is five in the *T. lanuginosus* structure, five in *Tr. reesei* I, four in *Tr. harzianum*, and 6 in *B. circulans*.

A detailed comparison with mesophilic family 11 xylanases (*51*) has revealed two other structural factors that contribute decisively to the observed thermostability, i.e., the existence of a disulfide bridge and electrostatic interactions.

The Disulfide bridge. There is one disulfide bridge in the *T. lanuginosus* enzyme which does not exist in the majority of other family 11 xylanases. It connects the C-terminus of the β-strand B9 (residue 110) with the N-terminus of the α-helix (residue 154). While a similar disulfide bridge probably also exists in the *Schizophyllum commune* xylanase (*80*), all other xylanases with known crystal structure have a hydrogen bond at the corresponding position.

Interestingly, attempts to enhance the thermostability of the *B. circulans* xylanase by introducing disulfide bridges via site-directed mutagenesis (*5*) have also targeted the topological equivalents of the two above residues. Together with two other disulfide bridges (a parallel one also connecting strand B9 with the helix plus one connecting N- and C-terminus), these mutations enhanced the thermostability by as much as 15 °C without, however, always improving the catalytic performance of the enzyme at elevated temperature. The crystal structure of such a *B. circulans* mutant reveals close similarity to the *T. lanuginosus* enzyme with respect to the conformation of the (left-handed) disulfide bridge. While it is thus beyond doubt that the disulfide bridge enhances the thermostability of the *T. lanuginosus* xylanase, other factors also have to contribute. This is evident from the fact that the *T. lanuginosus* enzyme outperforms with respect to its thermostability the above *Bacillus* mutant as well as the xylanase from *Schizophyllum commune*, despite 55% sequence homology and the presence of the S−S bridge in the latter protein.

Table 2: Number of Ion Pairs and Their Network Organization in a Variety of Xylanase Crystal Structures[a]

organism	no. of pairs	no. with $N=2$	no. with $N=3$	no. with $N=4$	no. with $N=5$	no. with $N=6$
T. lanuginosus	25	5	0	2	1	1
B. circulans	13	2	1	1	1	0
Tr. reesei I	11	2	0	2	0	0
Tr. reesei II	13	3	0	2	0	0
Tr. harzianum	14	2	1	1	1	1

[a] Two residues of potential opposite charge were considered an ion pair if their distance was below 8 Å.

Electrostatic Interactions. The result of a search for ion pairs and networks of ion pairs in the *T. lanuginosus* xylanase crystal structure as well as in structures of other family 11 xylanases is summarized in Table 2. Residues of opposite charges were assumed to form an ion pair if the distance between charged atoms was below 8 Å, without considering the dielectric properties of the environment. Evidently, the *T. lanuginosus* xylanase has the largest number of such ion pair interactions. This is illustrated in Figure 6, which compares the distribution of charged residues for the *T. lanuginosus* structure with xylanase II from *Tr. reesei*.

Residues of relevance for catalysis and for enzyme stability are expected to be conserved in related proteins. Indeed, the sequence alignment (Figure 1) reveals potentially charged residues to be conserved either near or within the active site (Glu 86, Arg 122, Glu 178) or quite far away, on the "opposite" side of the enzyme (Glu91, Asp111, Arg141, Arg145, His155; the latter, however, is most probably in an uncharged protonation state). There, they appear to stabilize an area of the enzyme which seems less well integrated into the compact β-sheet system of the protein scaffold. It is likely that this part of the protein, which contains a nine residue long loop connecting the helix with strand B4, is prone to unfolding and is therefore protected by a conserved ion-pair network. The sensitivity of this region of the molecule is supported by the observation of an intricate network of hydrogen bonds involving largely conserved residues (Ser139, His155, Tyr115, Asp111, Arg141, Trp159, Glu91) as well as a buried conserved water molecule (W204). In the *T. lanuginosus* xylanase, this apparently delicate region is further stabilized by three additional charged residues as well as by the disulfide bridge.

The thermostability of the *T. lanuginosus* xylanase is thus due to a disulfide bridge plus an extension of an existing network of charged residues, both stabilizing the most sensitive region of the molecule. Thermostability is further enhanced by an overall increase in the number of ion pairs, without targeting a specific area.

CONCLUSIONS

The structure of the xylanase from *T. lanuginosus* closely resembles the structures of other family 11 xylanases. The estimated pK_a values of the two active-site glutamates are consistent with Glu86 acting as the nucleophile and Glu178 acting as the acid−base catalyst. The fully conserved residue Arg122 stabilizes the negative charge on Glu86. Modeling studies of an enzyme−xyloheptaose complex indicate that only the three central sugar units (subsites, −2, −1, and +1) are rigidly bound. There is no room for this part of the substrate to carry substituents, while the other monomers may well be decorated. The thermostability of this xylanase is due to the presence of an extra disulfide bridge not observed in most mesophilic variants, as well as to an increase in the number of ion-pair interactions.

ACKNOWLEDGMENT

We thank J. Rouvinen for supplying us with the coordinates of the *Trichoderma reesei* xylanase II prior to their public release.

REFERENCES

1. Joseleau, J. P., Comtat, J., and Ruel, K. (1992) in *Xylans and Xylanases* (Visser, J., Beldman, G., Kusters, L., van Sommeren, M. A., and Voragen, A. G. J., Eds.) pp 1−16, Elsevier, New York.
2. Bedford, M. R., and Classen, H. L. (1992) in *Xylans and Xylanases* (Visser, J., Beldman, G., Kusters-van Sommeren, M. A., and Voragen, A. G. J., Eds.) pp 361−370, Elsevier, New York.
3. Maat, J., Roza, M., Verbakel, J., Stam, H., Santos da Silva, M. J., Bosse, M., Egmond, M. R., Hagemans, M. L. D., van Gorcom, R. F. M., Hessing, J. G. M., van den Hondel, C. A. M. J. J., and van Rotterdam, C. (1992) in *Xylans and Xylanases* (Visser, J., Beldman, G., Kusters-van Sommeren, M. A., and Voragen, A. G. J., Eds.) pp 349−360, Elsevier, New York.
4. Nissen, A. M., Anker, L., Munk, N., and Krebs-Lange, N. (1992) in *Xylans and Xylanases* (Visser, J., Beldman, G., Kusters-van Sommeren, M. A., and Voragen, A. G. J., Eds.) pp 325−338, Elsevier, New York.
5. Wakarchuk, W. W., Sung, W. L., Campbell, R. L., Cunningham, A., Watson, D. C., and Yaguchi, M. (1994) *Protein Eng. 7*, 1379−1386.
6. Harris, G. W., Pickersgill, R. W., Connerton, I., Debeire, P., Touzel, J. P., Breton, C., and Perez, S. (1997) *Proteins: Struct., Funct., Genet. 29*, 77−86.
7. McCarter, J. D., and Withers, S. G. (1994) *Curr. Opin. Struct. Biol. 4*, 885−892.
8. Sinnot, M. L. (1990) *Chem. Rev. 90*, 1171−1202.
9. Davies, G., and Henrissat, B. (1995) *Structure 3*, 853−859.
10. Rouvinen, J., Bergfors, T., Teeri, T., Knowles, J. K. C., and Jones, T. A. (1990) *Science 249*, 380−386.
11. Henrissat, B. (1991) *Biochem. J. 280*, 309−316.
12. Henrissat, B., and Bairoch, A. (1993) *Biochem. J. 293*, 781−788.
13. Derewenda, U., Swenson, L., Green, R., Wei, Y. Y., Morosoli, R., Shareck, F., Kluepfel, D., and Derewenda, Z. S. (1994) *J. Biol. Chem. 269*, 20811−20814.
14. Harris, G. W., Jenkins, J. A., Connerton, I., Cummings, N., Loleggio, L., Scott, M., Hazlewood, G. P., Laurie, J. I., Gilbert, H. J., and Pickersgill, R. W. (1994) *Structure 2*, 1107−1116.
15. Harris, G. W., Jenkins, J. A., Connerton, I., and Pickersgill, R. W. (1996) *Acta Crystallogr. D 52*, 393−401.
16. White, A., Withers, S. G., Gilkes, N. R., and Rose, D. R. (1994) *Biochemistry 33*, 12546−12552.
17. Dominguez, R., Souchon, H., Spinelli, S., Dauter, Z., Wilson, K. S., Chauvaux, S., Beguin, P., and Alzari, P. M. (1995) *Nat. Struct. Biol. 2*, 569−576.
18. Campbell, R. L., Rose, D. R., Wakarchuk, W. W., To, R., Sung, W., and Yaguchi, M. (1992) in *Trichoderma reesei Cellulases and Other Hydrolases* (Suominen, P., and Reinikainen, T., Eds.) pp 63−72, Foundation for Biotechnical and Industrial Fermentation Research.
19. Törrönen, A., and Rouvinen, J. (1995) *Biochemistry 34*, 847−856.
20. Törrönen, A., Harkki, A., and Rouvinen, J. (1994) *EMBO J. 13* (11), 2493−2501.
21. Schlacher, A., Holzmann, K., Hayn, M., Steiner, W., and Schwab, H. (1996) *J. Biotechnol. 49*, 211−218.
22. Gomes, J., Gomes, I., Kreiner, W., Esterbauer, H., Sinner, M., and Steiner, W. (1993) *J. Biotechnol. 30*, 283−297.
23. Gomes, J., Purkarthofer, H., Hayn, M., Kapplmüller, J., Sinner, M., and Steiner, W. (1993) *Appl. Microbiol. Biotechnol. 39*, 700−707.
24. Purkarthofer, H., Sinner, M., and Steiner, W. (1993) *Enzyme Microb. Technol. 15*, 677−682.
25. Purkarthofer, H., Sinner, M., and Steiner, W. (1993) *Biotechnol. Lett. 15*, 405−410.
26. Purkarthofer, H. (1993) Ph.D. Thesis, Institute of Biotechnology, Technical University of Graz, Austria.
27. Blum, M., Metcalf, P., Harrison, S. C., and Wiley, D. C. (1987) *J. Appl. Crystallogr. 21*, 235−242.
28. Kabsch, W. (1988) *J. Appl. Crystallogr. 21*, 67−71.
29. Kabsch, W. (1988) *J. Appl. Crystallogr. 21*, 916−924.
30. Bailey, S. (1994) *Acta Crystallogr. D 50*, 760−763.
31. Brunger, A. T. (1992) *X-PLOR, a System for X-ray Crystallography and NMR, Version 3.2*, Yale University Press, New Haven, CT.
32. Brunger, A. T. (1990) *Acta Crystallogr. A 46*, 46−57.
33. Jones, T. A., Zou, J. Y., Cowan, S., and Kjeldgaard, M. (1991) *Acta Crystallogr. A 47*, 110−119.
34. Brunger, A. T., Krukowski, A., and Erickson, J. W. (1990) *Acta Crystallogr. A 46*, 585−593.
35. Brunger, A. T. (1992) *Nature 355*, 472−474.
36. Engh, R. A., and Huber, R. (1991) *Acta Crystallogr. A 47*, 392−400.

37. Sheldrick, G. M. (1993) *SHELXL-93, a program for the refinement of crystal structures from diffraction data*, University of Göttingen, Germany.
38. Trueblood, K. N., Burgi, H. B., Burzlaff, H., Dunitz, J. D., Gramaccioli, C. M., Schulz, H. H., Shmueli, U., and Abrahams, S. C. (1996) *Acta Crystallogr. A 52*, 770−781.
39. Driessen, H., Haneef, M. I. J., Harris, G. W., and Holin, B. (1989) *J. Appl. Crystallogr. 22*, 510−516.
40. Laskowski, R. A., MacArthur, M. W., Moss, D. S., and Thornton, J. M. (1993) *J. Appl. Crystallogr. 26*, 283−291.
41. Yang, A.-S., Gunner, M. R., Sharp, K., and Honig, B. (1993) *Proteins: Struct., Funct., Genet. 15*, 252−265.
42. Windemuth, A. (1995) in *Parallel Computing in Computational Chemistry* (Mattson, T., Ed.) pp 151−169, ACS Symposium Series.
43. Brooks, B. R., Bruccoleri, B. D., Karplus, M., Olafson, D. J., States, D. J., and Swaminathan, S. (1983) *J. Comput. Chem. 4*, 187−217.
44. Sharp, K. A., and Honig, B. (1990) *Annu. Rev. Biophys. Chem. 19*, 301−332.
45. Nicholls, A., and Honig, B. (1991) *J. Comput. Chem. 12*, 435−445.
46. Tanford, C., and Roxby, R. (1972) *Biochemistry 11*, 2.
47. Plesniak, L. A., Connelly, G. P., Wakarchuk, W. W., and McIntosh, L. P. (1996) *Protein Sci. 5*, 2319−2328.
48. Joshi, M. D., Hedberg, A., and McIntosh, L. P. (1997) *Protein Sci. 6*, 2667−2670.
49. Wakarchuk, W. W., Campbell, R. L., Sung, W. L., Davoodi, J., and Yaguchi, M. (1994) *Protein Sci. 3*, 467−475.
50. Ha, S. N., Giammona, A., Field, M., and Brady, J. W. (1988) *Carbohydr. Res. 180*, 207−221.
51. Klintschar, G. (1997) Ph.D. Thesis, Department of Structural Biology, Institute of Physical Chemistry, Karl Franzens Universität, Graz, Austria.
52. Plesniak, L. A., Wakarchuk, W. W., and McIntosh, L. P. (1996) *Protein Sci. 5*, 1118−1135.
53. Keitel, T., Simon, O., Borriss, R., and Heinemann, U. (1993) *Proc. Natl. Acad. Sci. U.S.A. 90*, 5287−5291.
54. Wakarchuk, W. W., Sung, W. L., Campbell, R. L., Cunningham, A., Watson, D. C., and Yaguchi, M. (1994) *Protein Eng. 7*, 1379−1386.
55. Burmeister, W., Henrissat, B., Bosso, C., Cusack, S., and Ruigrok, R. (1993) *Structure 1*, 19−26.
56. Crennel, S. J., Garman, E. F., Laver, W. G., Vimr, E. R., and Taylor, G. L. (1993) *Proc. Natl. Acad. Sci. U.S.A. 90*, 9852−9856.
57. Miao, S. C., Ziser, L., Aebersold, R., and Withers, S. G. (1994) *Biochemistry 33*, 7027−7032.
58. Davoodi, J., Wakarchuk, W. W., Campbell, R. L., Carey, P. R., and Surewicz, W. K. (1995) *Eur. J. Biochem. 232*, 839−843.
59. McIntosh, L. P., Hand, G., Johnson, P. E., Joshi, M. D., Korner, M., Plesniak, L. A., Ziser, L., Wakarchuk, W. W., and Withers, S. G. (1996) *Biochemistry 35*, 9958−9966.
60. Gilbert, H. J., Hazlewood, G. P., Laurie, J. I., Orpin, C. G., and Xue, G. P. (1992) *Mol. Microbiol. 6*, 2065−2072.
61. van den Akker, F., Feil, I. K., Roach, C., Platas, A. A., Merritt, E. A., and Hol, W. G. (1997) *Protein Sci. 6*, 2644−2649.
62. DeDecker, B. S., R, O. B., Fleming, P. J., Geiger, J. H., Jackson, S. P., and Sigler, P. B. (1996) *J. Mol. Biol. 264*, 1072−1084.
63. Yamaguchi, S., Takeuchi, K., Mase, T., Oikawa, K., McMullen, T., Derewenda, U., McElhaney, R. N., Kay, C. M., and Derewenda, Z. S. (1996) *Protein Eng. 9*, 789−795.
64. Ko, J. H., Jang, W. H., Kim, E. K., Lee, H. B., Park, K. D., Chung, J. H., and Yoo, O. J. (1996) *Biochem. Biophys. Res. Commun. 221*, 631−635.
65. Ogasahara, K., Lapshina, E. A., Sakai, M., Izu, Y., Tsunasawa, S., Kato, I., and Yutani, K. (1998) *Biochemistry 37*, 5939−5946.
66. Auerbach, G., Huber, R., Grattinger, M., Zaiss, K., Schurig, H., Jaenicke, R., and Jacob, U. (1997) *Structure 5*, 1475−1483.
67. Voorhorst, W. G., Warner, A., de Vos, W. M., and Siezen, R. J. (1997) *Protein Eng. 10*, 905−914.
68. Hennig, M., Sterner, R., Kirschner, K., and Jansonius, J. N. (1997) *Biochemistry 36*, 6009−6016.
69. Wallon, G., Kryger, G., Lovett, S. T., Oshima, T., Ringe, D., and Petsko, G. A. (1997) *J. Mol. Biol. 266*, 1016−1031.
70. Salminen, T., Teplyakov, A., Kankare, J., Cooperman, B. S., Lahti, R., and Goldman, A. (1996) *Protein Sci. 5*, 1014−1025.
71. Villeret, V., Clantin, B., Tricot, C., Legrain, C., Roovers, M., Stalon, V., Glansdorff, N., and Van Beeumen, J. (1998) *Proc. Natl. Acad. Sci. U.S.A. 95*, 2801−2806.
72. Knegtel, R. M., Wind, R. D., Rozeboom, H. J., Kalk, K. H., Buitelaar, R. M., Dijkhuizen, L., and Dijkstra, B. W. (1996) *J. Mol. Biol. 256*, 611−622.
73. Watanabe, K., Hata, Y., Kizaki, H., Katsube, Y., and Suzuki, Y. (1997) *J. Mol. Biol. 269*, 142−153.
74. Macedo-Ribeiro, S., Darimont, B., Sterner, R., and Huber, R. (1996) *Structure 4*, 1291−1301.
75. Macedo-Ribeiro, S., Darimont, B., and Sterner, R. (1997) *Biol. Chem. 378*, 331−6.
76. Vogt, G., and Argos, P. (1997) *Folding Des. 2*, S40−S46.
77. Yip, K. S., Stillman, T. J., Britton, K. L., Artymiuk, P. J., Baker, P. J., Sedelnikova, S. E., Engel, P. C., Pasquo, A., Chiaraluce, R., and Consalvi, V. (1995) *Structure 3*, 1147−1158.
78. Delboni, L. F., Mande, S. C., Rentier-Delrue, F., Mainfroid, V., Turley, S., Vellieux, F. M., Martial, J. A., and Hol, W. G. (1995) *Protein Sci. 4*, 2594−2604.
79. Brocklehurst, S. M., and Perham, R. N. (1993) *Protein Sci. 2*, 626−639.
80. Oku, T., Roy, C., Watson, D. C., Wakarchuk, W., Campbell, R., Yaguchi, M., Jurasek, L., and Paice, M. G. (1993) *FEBS Lett. 334*, 296−300.
81. Barton, G. J., and Sternberg, M. J. E. (1987) *J. Mol. Biol. 198*, 327−337.
82. Barton, G. J. (1993) *Protein Eng. 6*, 37−40.
83. Livingstone, C. D., and Barton, G. J. (1993) *CABIOS 9*, 745−756.
84. Törrönen, A., Mach, R. L., Messner, R., Gonzales, R., Kalkkinen, N., Harkki, A., and Kubicek, C. (1992) *Biotechnology 10*, 1461−1465.
85. Yang, R. C. A., Mackenzie, C. R., and Narang, S. A. (1988) *Nucleic Acids Res. 16*, 7187.
86. Fukasaki, E., Panbangred, W., Shinmyo, A., and Okada, H. (1984) *FEBS Lett. 171*, 197−201.
87. Ito, K., Iwashita, K., and Iwano, K. (1992) *Biosci. Biotechnol. Biochem. 56*, 1338−1340.
88. Shareck, F., Roy, C., Yaguchi, M., Morosoli, R., and Klüpfel, D. (1991) *Gene 107*, 75−82.
89. Apel, P. C., Panaccione, D. G., Holden, F. R., and Walton, J. D. (1993) *Mol. Plant Microbe Interact. 6*, 467−473.
90. Zappe, H., Jones, W. A., and Woods, D. R. (1990) *Nucleic Acids Res. 18*.
91. Sakka, K., Kojima, Y., Kondo, T., Karita, S.-I., Ohmiya, K., and Shimada, K. (1993) *Biosci. Biotechnol. Biochem. 57*, 273−277.
92. Zhang, J. X., and Flint, H. J. (1992) *Mol. Microbiol. 6*, 1013−1023.
93. Paradis, F. W., Zhu, H., Krell, P. J., Phillips, J. P., and Forsberg, C. W. (1993) *J. Bacteriol. 175*, 7666−7672.
94. Kraulis, P. J. (1991) *J. Appl. Crystallogr. 24*, 946−950.
95. Merritt, E. A., and Murphy, M. E. P. (1994) *Acta Crystallogr. D 50*, 869−873.
96. Nicholls, A. J. (1993) *GRASP: Graphical Representation and Analysis of Surface Properties*, Columbia University, New York.

BI980864L